JOURNAL OF GEOPHYSICAL RESEARCH, VOL. 106, NO. A4, PAGES 6275–6289, APRIL 1, 2001

Spiky electric fields in the magnetotail

T. Streed,[1] C. Cattell,[1] F. Mozer,[2] S. Kokubun,[3] and K. Tsuruda[4]

Abstract. Large-amplitude spiky electric fields which have been proposed to provide energization and heating of particles have been observed in many regions of the magnetosphere, including the bow shock, auroral zone, and plasma sheet boundary. We extend previous statistical studies of such fields in the magnetotail (which were limited to $\lesssim 22\ R_E$) to cover the region explored by the Geotail satellite. Results are presented concerning the occurrence frequency, location, and association with density gradients of spiky electric fields in the magnetotail at radial distances of $\sim$10-200 R_E. Spiky fields do not occur beyond $\sim 100\ R_E$, and they predominantly occur at or near the plasma sheet boundary (as indicated by changes in the spacecraft potential) and are always associated with waves near the lower hybrid frequency. Spiky fields occur preferentially during periods of higher magnetic activity ($Kp > 3$). Statistical analysis of the direction of the largest field amplitudes provides information on the polarization of the waves and the spikes and therefore provides constraints on the origin of the fields. Waves which accompany the spikes are primarily polarized perpendicular to the magnetic field and are consistent with lower hybrid waves, while the spikes are polarized obliquely to the magnetic field. The results are described and compared with various possible generation mechanisms, including lower hybrid wave collapse, a leading candidate for explaining these spikes.

1. Introduction

The first observations of large spiky fields were made by the S3-3 satellite in the auroral zone at altitudes of approximately 1 R_E. These large electric fields were oriented primarily perpendicular to the magnetic field [*Mozer et al.*, 1977] and have been termed electrostatic shocks. Large spiky fields have also been observed in the plasma sheet boundary layer [*Cattell et al.*, 1982; *Wygant et al.*, 2000], the neutral sheet [*Cattell and Mozer*, 1982], the bow shock [*Wygant et al.*, 1987], and the magnetopause [*Cattell et al.*, 1995b]. In all of these regions it has been suggested that spikes could provide energization, heating, or dissipation. Spiky electric fields are large amplitude, often over an order of magnitude larger than the background convection or wave electric field, and are short duration (of the order of 0.1 s) and are not periodic structures. The first detailed statistical study of spikes in the magnetotail was done by *Levin et al.* [1983] using ISEE data for radial distances of 7-23 R_E. *Levin et al.* [1983] found that the occurrence and magnitude of the spiky fields observed were not inconsistent with the mapping of electrostatic shocks from lower altitudes. *Cattell et al.* [1994] examined several examples obtained by Geotail at radial distances of 40-90 R_E and found that the spikes were often superimposed upon lower hybrid drift waves which tended to occur in short packets of a few seconds to tens of seconds.

The purpose of this study is to extend earlier work by performing a large statistical analysis encompassing the magnetotail from 10 R_E to 200 R_E. A key purpose of this study is to determine the origin of spiky electric fields. The three leading theoretical mechanisms which could produce spiky electric fields are lower hybrid drift wave collapse, the mapping of low-altitude electrostatic shocks, and kinetic Alfvén waves. Each of these theories predict specific characteristics of the fields which can be compared with the actual satellite data to ascertain which mechanism is correct.

A better understanding of these fields is important owing to their probable importance in magnetotail dynamics. In other regions of the magnetosphere, it has been shown that the spikes energize and heat particles. For example, *Temerin and Cravens* [1990] showed that random electric field "spikes" at lower altitudes could explain electron conics, energized electrons peaked at

[1]School of Physics and Astronomy, University of Minnesota, Minneapolis, Minnesota.
[2]Space Sciences Laboratory, University of California, Berkeley, California.
[3]Solar-Terrestrial Environmental Laboratory, Nagoya University, Taoyokawa, Japan.
[4]The Institute of Space and Astronautical Science, Sagamihara, Japan.

Paper number 2000JA900154.
0148-0227/01/2000JA900154$09.00

angles oblique to the magnetic field. *Borovsky* [1984], using test particle simulations, found that double layers with the electric field at oblique angles to the background magnetic field could produce ion conics, beams of ions whose pitch angle distributions have minima in the field-aligned direction. Presently, we are studying ion dynamics in the magnetotail by using a particle tracing code which has been supplemented by a model of spiky electric fields based upon the statistical results presented herein. Preliminary results indicate that these fields dramatically modify individual particle trajectories, result in particle energization, and modify particle distributions, in both configuration and velocity space. Previous studies have also shown that the presence of lower hybrid waves, which the spikes seen in this study are always embedded upon, result in greater energization of ions [*Cattell et al.*, 1995a, 1996] and are important in magnetotail dynamics [*Cattell and Mozer*, 1986, 1987, K. Sigsbee et al., manuscript in preparation, 2001].

It is also important to understand the origin of these fields. If spiky electric fields are the mapping of electrostatic shocks, which have been shown to accelerate auroral particles (see, for example, *Temerin and Mozer* [1987] and *McFadden et al.* [1999]), then these fields are a link between auroral phenomena and distant tail activity. If these fields are due to lower hybrid collapse, they provide evidence for collapse in a vastly different regime than previous ionospheric observations of collapse, which suggests the need for more theoretical and simulation work, specifically addressing magnetotail parameters.

The outline of this paper is as follows: in section 2, the three possible theoretical mechanisms for these spikes will be discussed, emphasizing empirical tests which separate these alternatives. This discussion will be followed by a brief introduction to the Geotail spacecraft orbit and instrumentation in section 3, the event selection process for the statistical database in section 4, and the methodology behind the statistical study in section 5. The main focus of sections 6 and 7 will be results of the spike analysis. Section 6 will cover more general results, emphasizing their location, corresponding magnetic activity, their polarization angles with respect to the magnetic field, and the frequency of the surrounding waves. Section 7 will examine the empirical tests outlined in section 2 in more detail. Section 8 follows, with conclusions drawn about these spikes and future work to be performed.

2. Theoretical Mechanisms

To complete an analysis of the data, the experimental results must be compared with theoretical mechanisms regarding the origin of these fields. Each of the three leading candidates will be discussed below with particular emphasis upon theoretical criteria which can be compared with the satellite data.

2.1. Mapping of Electrostatic Shocks

Electrostatic shocks [*Mozer et al.*, 1977; *Mozer and Kletzing*, 1998] are found to be oriented primarily perpendicular to the magnetic field. Initial work was done at altitudes of 1000-8000 km in the auroral zone. *Mozer* [1981], using ISEE1 data, showed that electrostatic shocks were found at all distances up to 7 R_E. Assuming that the shocks are electrostatic and that magnetic field lines are electric equipotentials, they will map along field lines with an amplitude that falls off roughly as $\sqrt{B}$. Along the high-altitude extension of auroral field lines, electric fields oriented primarily perpendicular to B with reduced amplitudes should be seen. In addition, since electrostatic shocks are excited near ~ 1 R_E on auroral field lines, these fields will not be seen on magnetic field lines which are not connected to the auroral zone. If these auroral field lines are closed, they will not be seen beyond the distant x line, at ~ 100 R_E. To test this amplitude mapping, *Levin et al.* [1983], in a statistical study of large electric field events using ISEE1 data with radial distances out to 22 R_E, found that the large electric fields were not inconsistent with the mapping of electrostatic shocks along equipotential field lines to the plasma sheet boundary layer in the magnetotail. *Levin et al.* [1983] also found that the probability of observing these fields was largest near dusk, in agreement with lower-altitude shocks (see, for example, *Redsun et al.* [1985]).

This model has several predictions which can be checked with the Geotail data set to test its validity. The mapping of electrostatic shocks along closed magnetic field lines implies that spikes should usually not be seen beyond ~ 100 R_E (the average location of the distant neutral line). The amplitude of the electric field should fall off as $\sqrt{B}$. Lastly, this theory suggests that the spikes should be electrostatic and not electromagnetic. It should be noted that the greater probability of observing these structures near dusk is difficult to study in the magnetotail owing to the uncertainties inherent in mapping to such large distances.

2.2. Kinetic Alfvén Waves

The shear Alfvén wave is modified by kinetic effects, including finite electron pressure and finite ion gyroradius, resulting in a new dispersion relation for kinetic Alfvén waves (see, for example, *Lysak and Lotko* [1996] and references therein). Kinetic Alfvén waves give rise to parallel electric fields which can accelerate particles. It has been suggested that the spikes seen in the magnetotail may be the electric field signature of a kinetic Alfvén wave. In addition, *Lysak and Dum* [1983] and *Lysak* [1998] suggest that at lower altitudes these waves may form the electrostatic shocks described in the last section. In this case we are dealing with a wave in which k is primarily parallel to the magnetic field and which is electromagnetic instead of electrostatic. Thus electric and magnetic field fluctuations are required to match

the dispersion relation given by *Lysak* [1998]. Kinetic Alfvén waves have been observed in the auroral zone at altitudes near 1 R_E [*Louarn et al.*, 1994] and at the plasma sheet boundary at radial distances of 4-6 R_E (J. Wygant et al., Evidence for kinetic Alfvén waves and parallel electron energization at 5-7 R_E altitudes in the plasma sheet boundary layer, submitted to *Journal of Geophysical Research*, 2000).

There are three major constraints provided by this theory which may be tested. Now that the spikes are electromagnetic instead of electrostatic, magnetic fluctuations are necessary. The amplitudes of the electric and magnetic field fluctuations need to match the dispersion relation as given by *Lysak* [1998]. A normalization condition has been derived which can also be compared to the data in a manner similar to the electrostatic shocks described earlier (this will be discussed further in section 7.2).

2.3. Lower Hybrid Drift Waves and Wave Collapse

The lower hybrid drift wave is an electrostatic low-frequency wave with its wave vector primarily perpendicular to the magnetic field [*Huba et al.*, 1978, and references therein]. It is characterized by magnetized electrons and unmagnetized ions so that the electron equation of motion requires the $v \times B$ term, while the ion equation does not contain this term. The instability is driven by cross-field current due to a density gradient. Lower hybrid waves have previously been identified in the magnetotail [*Cattell and Mozer*, 1986, 1987; *Cattell et al.*, 1994; *Okada et al.*, 1994; *Shinohara et al.*, 1998, K. Sigsbee et al., manuscript in preparation, 2001]. It has been suggested that when the wave amplitude becomes large enough, the ponder motive force will give rise to density "potential wells" which trap particles. Then owing to a wave-wave interaction, these waves collapse. The end result of this collapse is the nonlinear growth of the waves and spikes. In this case, *Shapiro et al.* [1993] give the following condition on electric field amplitudes needed to produce collapse:

$$\frac{E^2}{4\pi n T_e} > \frac{m_e}{M_i}\left(\frac{\omega_{ce}}{\omega_{pe}}\right)^2 (k\rho_e)^2, \qquad (1)$$

where ω_{ce} is the electron cyclotron frequency, ω_{pe} is the electron plasma frequency, and ρ_e is the electron gyroradius. If this theory provides the explanation for the generation of spiky electric fields, the wave vector k should lie mainly perpendicular to B, though it can have a small parallel component. *Huba et al.* [1978] have also placed constraints upon the ratio of $k_{\|}$ over $k_{\perp}$ for the waves surrounding the spikes. In addition, if the observed spikes are due to the collapse of lower hybrid drift waves, then the spikes need to be embedded in a region of lower hybrid waves, and the waves need to often meet the amplitude threshold given above. *Cattell et al.* [1994] showed that this threshold was met for some Geotail events.

This theory can be tested by determining whether (1) the spikes usually occur within a region of lower hybrid waves and (2) the electric field amplitudes match the condition in equation (1). Note that testing the first condition requires distinguishing between the identification of the lower hybrid waves and the spikes.

3. The Geotail Spacecraft

3.1. Orbit Information

The Geotail satellite was launched in July 1992 for the specific purpose of studying the dynamics and structure of the magnetotail [*Nishida*, 1994]. The orbit of Geotail consisted of several deep-tail passes between 1992 and 1994, whereupon the apogee was moved inward. Events from January 1993 through March 1997 are included in this statistical analysis, covering radial distances from 10 R_E to 200 R_E. Since one of the critical elements in this study is an analysis of the location where these spiky fields occur, it is crucial to carefully analyze coverage obtained during this 4-year period. For plots showing Geotail's orbit, see *Nishida* [1994] and *Matsumoto et al.* [1998]. Coverage is quite good inside 30 R_E but does contain gaps at larger radial distances. Analysis of the locations of the spiky field events described below, normalized by the coverage of Geotail at that location, shows that most of the events occur between 20 and 50 R_E and that no events occur beyond 100 R_E.

3.2. Instrumentation

In this study, data from both the Geotail electric field detector (EFD) [*Tsuruda et al.*, 1994] and the onboard fluxgate magnetometers [*Kokubun et al.*, 1994] have been utilized. Understanding the nature of the electric field instrument is crucial to this study. The electric field instrument consists of a pair of booms with spherical sensors spinning in the ecliptic plane and therefore provides a two-dimensional measurement of the electric field every spin period or, instantaneously, the component of the electric field along the boom direction. Thus instead of a direct three-dimensional comparison of the direction of the electric field relative to the direction of the geomagnetic field, it is necessary to do any polarization studies statistically. A detailed description of how this is accomplished is presented in the methodology section below. The EFD samples at a rate of 32 points a second, placing an upper frequency limit of 16 Hz upon any power spectra of the electric field. Since lower hybrid waves are a crucial element to this discussion, it must be noted that often the lower hybrid frequency is below the 16-Hz threshold, but for events in the inner magnetotail, the lower hybrid frequency often is greater than 16 Hz. Also note that the raw electric field data are modulated by the 3-s spin period

of the spacecraft, assuming a constant dc field over the 3-s spin period. A filter is applied to remove the spin periodicity from the data.

In addition, the spacecraft potential is used to provide an estimate of density, based upon the work of *Pedersen* [1995]. Note that *Ishisaka et al.* [1999] found, using Geotail data, that spacecraft potential was a good measure of density for potentials of less than 35 V, which implies ranges of electron density above 0.02 cm^{-3}. *Ishisaka et al.* [1999] also showed that the spacecraft potential was useful for measuring the density in both the plasma sheet and the plasma sheet boundary layer, which is the region of interest for this paper. In addition, for the purposes of this study we are most interested in changes in density, not the actual density values; so any limitation in the absolute calibration of the density estimate is of minimal concern.

4. Event Selection

The events for this study were chosen on the basis of the calculation of the standard deviation of the spin fit of the electric field. If the variance was found to be greater than 0.6 for 10 or more consecutive data points, the interval was chosen as a possible time for consideration. This criterion selects for intervals with large electric fields variations on the periods of less than 3 s. The resulting database contains 178 events (211 hours of data). The value 0.6 was chosen arbitrarily on the basis of initial trials. Although the selection of a particular value of the variance is arbitrary, choosing a differing value would simply change the number of events in the statistical database and not the results. To verify this conjecture, lower variance values were examined. The resulting database contained the 178 events plus additional events. These additional events contained spiky electric fields; however, the amplitudes were greatly reduced, and so they could be excluded from the study. Each candidate time was then examined by eye, to set the exact starting and ending times. Thus for the purposes of this study, an event is defined as a period from 30 min to 2 hours which includes packets of large-amplitude spikes which meet the criteria described above along with intermittent periods of quieter electric fields. An example (Figure 1) shows 1 hour of data (1730-1830 UT) for January 30, 1995, when Geotail was at [-36, 4, -4] R_E in GSE coordinates. The panels show B_x, B_y, B_z in GSE coordinates, the magnitude of the electric field along the spinning booms, and the negative of the spacecraft potential. The spiky fields are easily apparent, having a larger amplitude than the background field, sometimes extending to above 50 mV/m in this example. A vertical line has been added at 1755 in the electric field and spacecraft potential panels to highlight that the largest-amplitude spikes correspond with the largest changes in the spacecraft potential (largest changes in the density). This

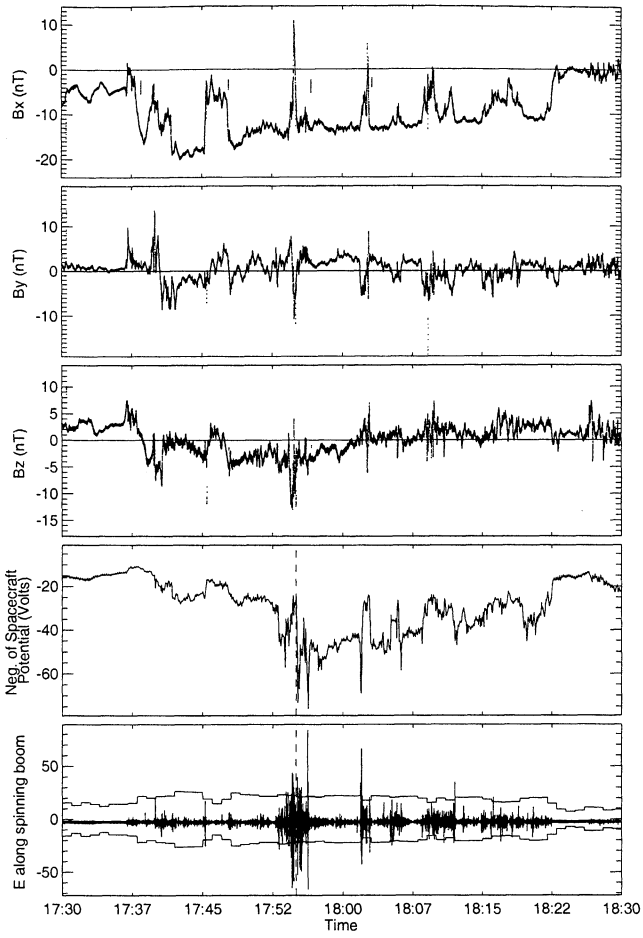

Figure 1. A typical event for the statistical study. This event occurs at [-36, 4, -4] R_E (GSE coordinates) at 1730-1830 UT on January 30, 1995. Panels show three components of the magnetic field, negative of the spacecraft potential, and electric field along the spinning booms. Note the large spiky fields. The vertical dashed line shows the correspondence of changes in the spacecraft potential (a rough measure of density [*Pedersen*, 1995]) and the spiky electric fields, which is discussed later. The jagged horizontal lines in the bottom panel correspond to the same critical value used in Figure 6 and show how one can select data points that consist of spikes and not the waves the spikes are embedded upon.

correspondence can be seen throughout the entire hour of data, as times with more spikes are times with large density changes. The importance of the effects of density gradients will be discussed further in section 6.4. The jagged horizontal lines added to the bottom panel represent a critical value which is used to select a subset of the electric field points for analysis and will be described in more detail in section 6.3. Note that the method used to select events was a priori independent of spacecraft position; however, the resulting data set shows a definite dependence on radial distance. The absence of any events beyond 100 R_E confirms this, and it will be discussed further below.

5. Methodology

One important goal of this study was to analyze the polarization of the waves and determine whether the large electric field spikes occur predominantly at specific angles with respect to the magnetic field, as this information helps ascertain the origin of the spiky fields. The polarization is determined by finding the angle between the electric field and magnetic field for both the case of all the spin-filtered electric field points (which samples primarily waves) and then specifically for spiky electric fields. As was stated previously, because of the limitations of the electric field instrument, this is done statistically. The procedure is as follows: For each data point, the angle between the instantaneous electric field along the boom, $E_{\text{alongboom}}$, and the total magnetic field $\vec{B}$ (called phi) is calculated, along with the angle between $E_{\text{alongboom}}$ and B_{xy} (called theta), where B_{xy} is the component of the magnetic field in the ecliptic plane. Both calculations are necessary, since Geotail only measures the component of the electric field in the spin plane. Thus a large B_z component would result in an angle that was always around 90°. This is illustrated in Figure 2. The raw electric field is used to achieve higher time resolution, because it samples at a rate of 32 points per second along the spinning booms. Note that all analysis is performed on data which have been filtered first at the 3-s spin period of the spacecraft to remove the quasi-static electric field. The resulting calculated angle is binned, each bin corresponding to 20° (0°-20°, 20°-40°, etc.). Each bin is normalized by dividing by the total number of counts in that bin obtained by including all data points. This eliminates any bias due to sampling. If the predominant angles are found to lie close to 90°, then the component of the spiky electric field in the spin plane is on average primarily perpendicular to the magnetic field; if the angles are mainly near 0°or 180°, then the electric field is parallel to the magnetic field. The electric field probe completes one revolution in 3 s, and assuming that the magnetic field does not change direction within that same period, a data set which examines every point will not show any preferential direction, since every angle receives equal "coverage." However, examining electric field points with a magnitude greater than some threshold affords the opportunity to see if these larger-amplitude spikes have a preferred direction relative to the field. Both of the resulting polarization plots (Figures 5 and 6) have the same form. The top panel shows the fraction of counts for the theta angle, in 20° bins. If all data points were examined, each theta bin would contain an equal number of counts, and the fraction of counts would equal one, as was explained above. The second panel shows the number of counts for the phi angle, again in 20° bins. Examining all data points will not result in equal coverage for each bin, since any B_z component will favor angles toward 90° and eliminate angles near 0°. The larger this component, the stronger this effect becomes.

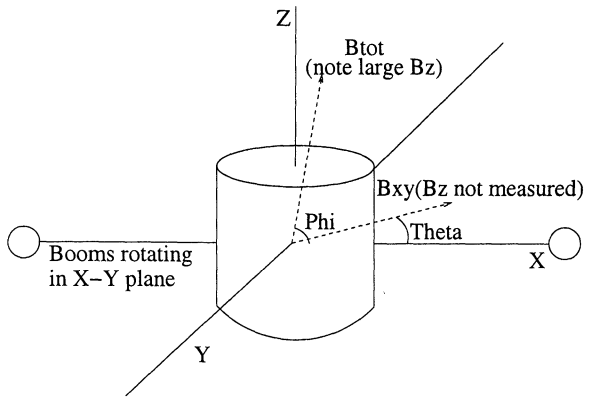

Figure 2. Diagram showing the two angles measured in the statistics. Theta measures the angle between the booms and the B_{xy} component (the component in the ecliptic plane), while phi measures the angle between the booms and the total magnetic field vector. Note that a large B_z component ensures a large phi angle, since the spin plane is solely in the x-y plane. To compensate for this, times were examined where B_z was not the largest component of the magnetic field. Also note that since theta samples all angles during a 3-s period, it will measure an equal number of points at every angle. Only when selecting a subset of the data points (based upon the amplitude of the points) will any angular dependence be seen in theta.

6. General Results

6.1. Location

The resulting database consisted of events throughout the magnetotail, from 10 to 100 R_E in X_{gse}, from -20 to 20 R_E in Y_{gse}, and from -10 to 10 R_E in Z_{gse}. Taking into account the increased satellite coverage for events inside 40 R_E results in more events between 20 and 50 R_E. No events are found beyond $\sim$ 100 R_E. The lack of events beyond 100 R_E strongly suggests that spiky fields do not occur beyond the distant x line. The mapping of electrostatic shocks would be consistent with this observation, since the spiky electric fields would only occur on magnetic field lines which map to the auroral zone. To verify the lack of any events beyond 100 R_E, the variance value was lowered to 0.3 to search for possible events during deep-tail (> 100 R_E) passes. Only six events were found, and upon visual inspection, the large fields were found to be either dc fields or bad data points. Since no spiky field events were found even for a lower variance value, it is very likely that these fields do not occur beyond 100 R_E. It should also be noted that the magnitudes of the spikes become smaller at larger radial distances. This is illustrated in Figure 3, which displays the three largest electric field values per minute for each of the 178 events versus the corresponding radial distance.

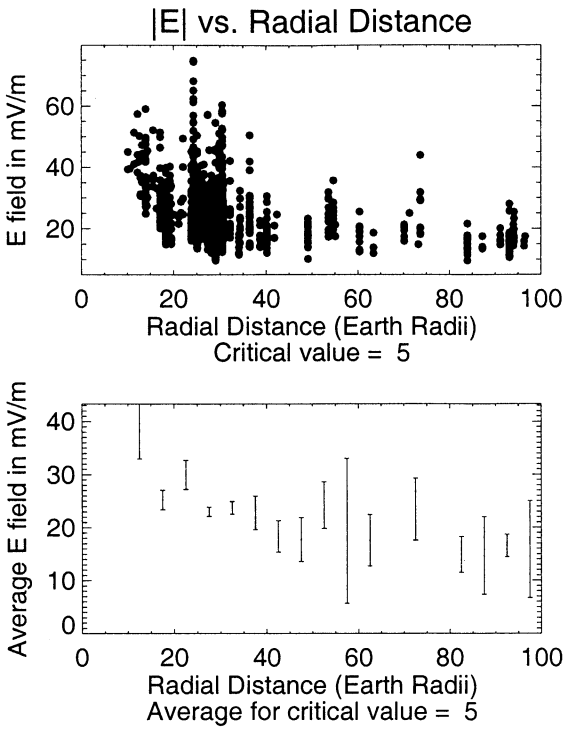

Figure 3. Magnitude of each filtered electric field data point versus their corresponding radial distance. (top) Largest electric field points versus radial distance; (bottom) averages of all the data points with amplitudes > 5 mV/m in 5 R_E bins. Note that the amplitudes appear to fall off with greater radial distance, for both the largest spike amplitudes and the averages. The larger number of data points between 20 and 40 R_E is partially due to the orbit of the Geotail satellite.

6.2. Magnetic Activity

To determine whether spiky fields and large-amplitude waves occur preferentially during periods of larger magnetic activity, we have examined the Kp values during these events. Figure 4 shows the Kp data for the 178 events, normalized by dividing by all Kp data for 1993-1997. Note that the majority of the events occur when $Kp > 3$, which shows a strong correspondence between active times and spiky electric fields.

6.3. Polarization Angles

As was stated previously, a key element of this study is the analysis of the polarization of the waves and the spikes. The simplest procedure is to bin all electric field points above a certain threshold amplitude by their polarization angle, looking for any preferential angle in the distribution. The top two panels of Figure 5 show plots for all electric field points greater than 5 mV/m and the corresponding angle between the electric field and magnetic field. This threshold includes all the spikes in the study and many of the waves which are colocated with the spikes. Both Figures 5 and 6 are normalized as described in section 5 to eliminate any preferential angle dependence due to the background magnetic field direction or other effects. The top two panels of Figure 5 show a clear predominance of angles near 90°, suggesting that the polarization is perpendicular. This is in clear agreement with lower hybrid waves, for which the wave vector is primarily perpendicular to the magnetic field. In contrast, the bottom two panels of Figure 5, which include only points with an amplitude > 40 mV/m, shows that the largest number of counts are at angles oblique to the magnetic field. This implies that the spikes have components both parallel and perpendicular to the magnetic field.

Figure 5 may be biased by the fact that the magnitude of spikes is highly dependent upon radial distance, as was shown in Figure 3. Since spike amplitude is not constant with radial distance, the above analysis strategy will include more events from regions closer to the Earth. One possible remedy is to normalize by the strength of the magnetic field. Note that this normalization scheme is that expected for the mapping of electrostatic shocks along equipotential field lines; however, this normalization also allows for a better comparison with the results of *Levin et al.* [1983] and with the consistency of the results obtained from different normalization mechanisms. Now instead of using the amplitude of the electric field as the threshold value, we introduce a critical value to measure the threshold value. The critical value can be written mathematically as

$$\text{critical value} \leq \frac{\text{spike(mV/m)}}{\sqrt{B}}. \qquad (2)$$

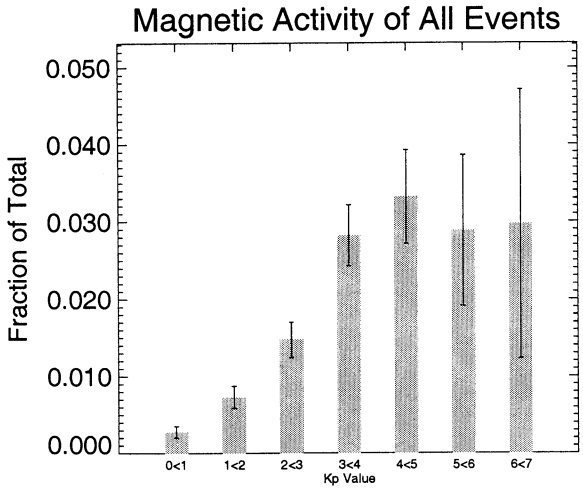

Figure 4. Spiky electric fields which take place predominantly during active times. This plot shows the number of events in the data set which have the corresponding Kp values, normalized by dividing by all Kp values for 1993-1997. The orbit of Geotail may introduce a slight bias in that Geotail is more likely to cross the plasma sheet boundary during active times, yet this plot still shows that most events have $Kp > 3$, which says the spiky field events correspond with times of high magnetic activity.

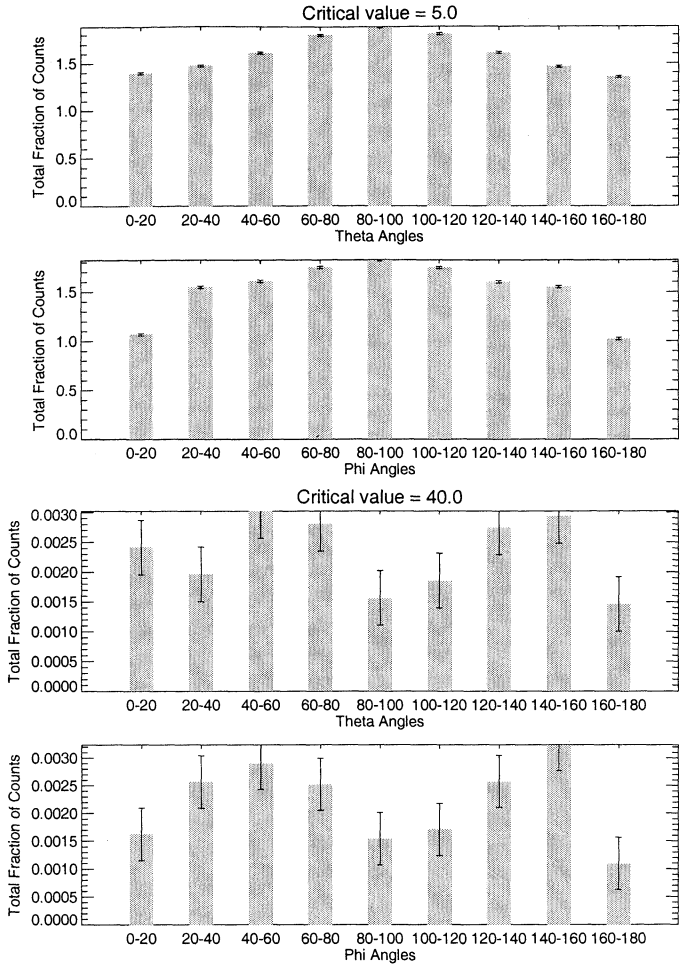

Figure 5. Histogram of relative angle between magnetic and electric field. The top two panels are for all electric field points with an amplitude > 5 mV/m. The largest bins are near 90°, which implies perpendicular polarization. The bottom two panels are identical except now only for electric field points with an amplitude > 40 mV/m. Note that the top two panels include both the spikes and the waves they are embedded upon, while the bottom two panels show only the spikes. Now the largest bins are near 45°, which implies an oblique angle polarization, including both parallel and perpendicular components. The same analysis seen here has been performed on events where $B_z < 5$ nT and where $B_z/\sqrt{B_x^2 + B_y^2} < 0.2$ to focus on events when B_z is small, and the same result is found.

Examples of binning using this normalization are shown in Figure 6. The top two panels of Figure 6 show all electric field points with a critical value > 1.0, which corresponds to ~ 5 mV/m for a local magnetic field of ~ 25 nT. This corresponds to a case where both large spikes and the surrounding waves are included. In contrast, the bottom two panels of Figure 6 are for a larger critical value and thus solely examines spikes. The electric field amplitudes corresponding to this critical value are shown by the horizontal jagged lines in Figure 1 as an example (note that this value changes with the magnetic field). The results are similar to the results obtained by binning by electric field amplitude, although the enhancement at oblique angles is less pronounced. For lower critical values, the polarization is primarily perpendicular; for larger critical values, more of the electric field points lie at oblique angles.

Because the electric field in the z direction is not measured, it is important to study times when the B_z component was small. By analyzing events where the B_z component was negligible, one selects events where the polarization of the electric field component in the spin plane can be determined. This is done by two different methods. The first method was to look at events where $|B_z| < 5$ nT compared with times when $|B_z| > 5$ nT. The second method was to bin by the ratio of the B_z magnitude compared with the B_x and B_y magnitudes. Small B_z events were defined to be when this ratio was < 0.2. The results of these binnings were identical to those shown in Figures 5 and 6. Additional binning was also performed by the sign of the B_x component, to look for any dependence upon whether the spacecraft was above or below the neutral sheet. No dependence was found. Note that no information about the polar-

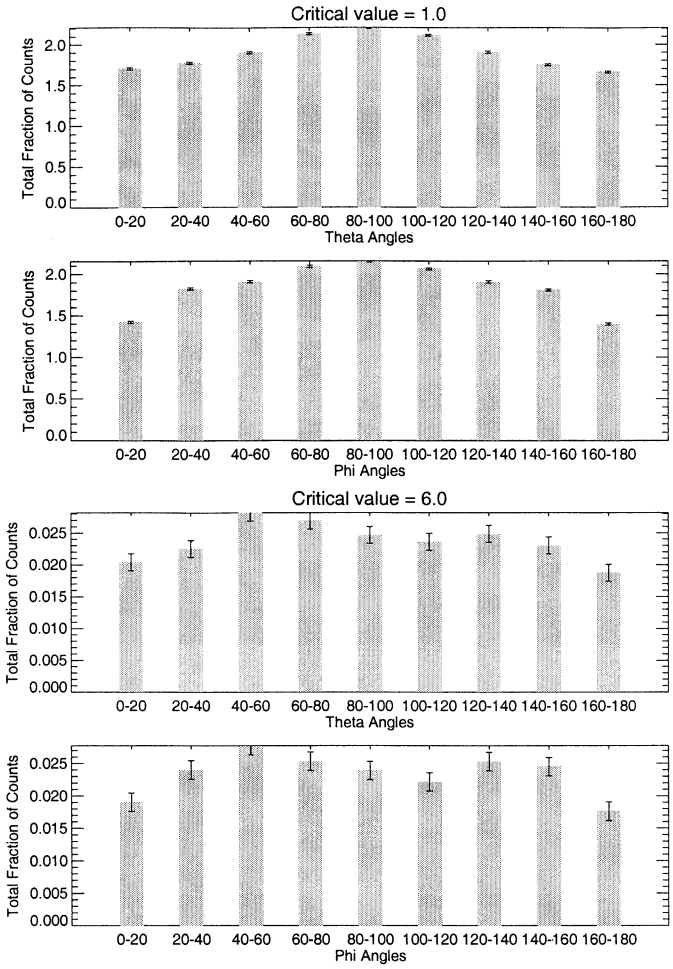

Figure 6. Top two panels, histogram plots for polarization for electric field points with a critical value > 1.0. Perpendicular angles dominate. Bottom two panels, points with a critical value > 6.0. Note the oblique angle dominance.

ization of the z component of the electric field can be obtained.

It is also important to determine whether the polarization changes with radial distance. In other words, are the polarization results different for events at 20 R_E than at 80 R_E? This can be done by comparing data in 20 R_E bins for the various binning strategies described above. Examination reveals no trends with radial distance. The same predominance of perpendicular angles for lower critical values for lower amplitudes and oblique angles for higher critical values is seen equally at all radial distances.

6.4. Density Gradients

Previous studies have concluded that spiky electric fields are often found at or near the plasma sheet boundary (PSB) [*Cattell et al.*, 1982; *Levin et al.*, 1983]. One straightforward method for ascertaining whether these spikes are found in or near the PSB is to look for large changes in the density, which is a clear indicator of Geotail traveling into the PSB from the lobe or the plasma sheet. Therefore occurrence frequency of spiky electric fields was binned by density gradients. For example, by examining the spacecraft potential data in Figure 1, one can see that Geotail was originally in the plasma sheet but did cross the PSB multiple times, as can be seen by the large changes in the spacecraft potential (or density). Also note that the largest electric field amplitudes (the spikes) in Figure 1 correspond to the times when the spacecraft potential was going through its largest changes. It should be noted that sometimes the spikes are found during neutral sheet crossings which also have changes in the density. This is also apparent in Figure 1. To examine whether these effects hold throughout the entire data set, electric field points with various critical values were binned according to the density changes seen in the same minute of data. Note that this binning assumes that the plasma sheet boundary velocity with respect to the spacecraft was not very different from event to event. An example of this type of plot is shown in Figure 7. The top panel shows all electric field points binned by density changes on a logarithmic scale. This includes all data, including times with spikes and times which precede or follow spikes. Contrast this

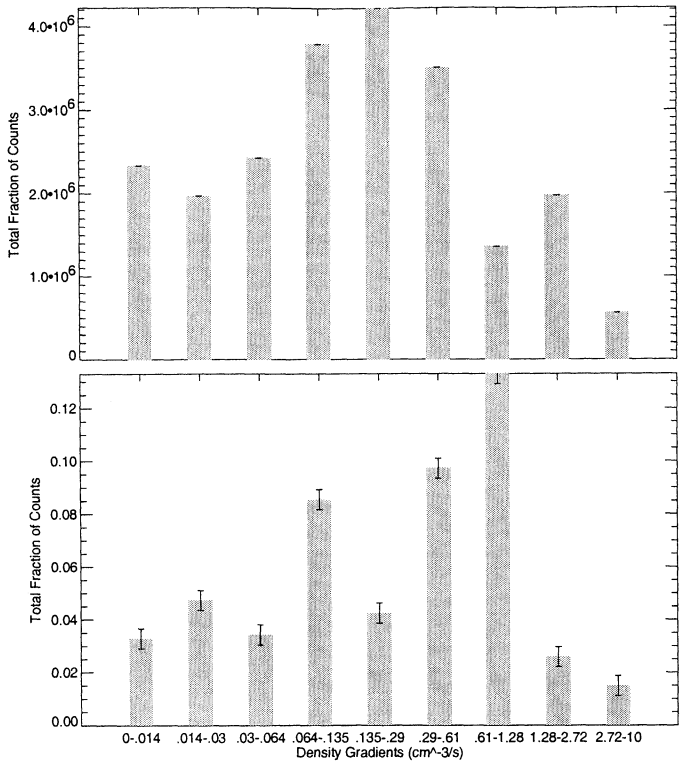

Figure 7. Correspondence between times with spiky electric fields and changes in the density, another key element to the study. This can be seen in Figure 1 by the dashed line. This was seen in all the events and so was studied more carefully. (top) Changes in the density (on a logarithmic scale) for all electric field data points in the study. (bottom) Changes only for minutes of data containing points above the critical value = 4.0 threshold (same normalization procedure as was used in Figure 10). Note the shift in the data to the right, signifying that times containing stronger spikes tend to correspond to times of larger density changes.

with the bottom panel of Figure 7, which shows only the electric field points with a critical value larger than 4. The bottom panel is normalized by dividing all bins by the critical value = 0 results (all data points, i.e., by the top panel), which removes any trends except those due to looking at times containing stronger spikes versus including times where there are no spikes or weaker spikes. The bottom panel shows that more spikes occur during periods of larger density changes. The fact that not many spikes occurred during the very largest density gradients may partly be explained if these large density gradient values are actually due to rapidly moving boundaries rather than true gradients. The data set was also examined by hand to test the correspondence between large density changes and spiky fields. In 100% of the events examined, times when large spiky fields occurred corresponded with large density gradients. In 40% of the events examined, there were large density gradients which contained no spiky electric fields.

6.5. Simulation of Probes

One of the inherent difficulties in the polarization results is the lack of a three-dimensional measurement of the electric field by Geotail which requires the use of statistical studies. To determine whether the polarization of the spin plane electric field was correctly determined, a simple computer simulation of the electric field probes on Geotail was designed, and results of these simulations were compared with the actual data. By using polarization results obtained from the simulation with known electric and magnetic fields, we could determine if the histogram plots were being interpreted correctly.

A pair of "virtual booms" were constructed to spin in the ecliptic plane. A fully three-dimensional magnetic field and electric field are used. The magnetic field is constructed as having x, y, and z components which are constant but can have different initial values. Thus they can be modeled after specific Geotail events or can be configured on the basis of the average geomagnetic field in the tail. The electric field is constructed in two parts, a very small background field and a large spiky field which is centered in the k direction. The amplitudes of these fields vary, and k can be picked to lie in any direction, with particular interest in the perpendicular and parallel directions (relative to the magnetic field). A small δk is selected as well to allow the input electric field to have a small spread in direction. Various con-

figurations of differing k vectors and magnetic fields are chosen and then compared with the data. This is an excellent diagnostic of how well the statistical results are understood. The virtual booms "spin" through these fields, and the angle is calculated between the magnetic field and the component of the electric field which lies in the direction of the booms. A threshold value is added to only examine larger electric fields, as was described previously.

Although this simulation is quite simple, results are in general agreement with the data, in that using an input of spikes which lie primarily perpendicular to the magnetic field with a small parallel component results in very similar looking histograms to what is seen by using the Geotail data set.

6.6. Identification of Lower Hybrid Waves

The presence of lower hybrid waves in the magnetotail has previously been established [*Cattell and Mozer*, 1986, 1987; *Okada et al.*, 1994; *Shinohara et al.*, 1998]. *Cattell and Mozer* [1986, 1987], using ISEE data, showed that both the frequency and wavenumber of observed waves were consistent with lower hybrid waves. *Okada et al.* [1994], in two passes of Geotail through the plasma sheet boundary layer, found quasi-monochromatic waves in the lower hybrid frequency range. More importantly, *Okada et al.* [1994] found no fluctuating magnetic field component larger than 1 pT and calculated E/B ratios consistent with phase velocities of $> 10^6$ km/s, which indicates that the observed waves were primarily electrostatic. *Shinohara et al.* [1998], in a study of four Geotail encounters with the neutral sheet at radial distances of 10-30 R_E, also found lower hybrid turbulence. *Shinohara et al.* [1998] did find an electromagnetic component of the order of a few nanoteslas and calculated E/B ratios consistent with phase velocities of $5 \cdot 10^3$ - 10^5 km/s and concluded that the observed turbulence was in good agreement with the linear theory for the lower hybrid drift instability, including effects of magnetic curvature.

In order to determine the magnetic components which might be associated with the waves and the spikes, a subset of nine large electric field events were examined. During intervals with waves near the lower hybrid frequency in the electric field, magnetic field fluctuations were sometimes observed. The magnitude was usually a few tenths of a nanotesla, and was always less than 1 nT. This is consistent with previous observations [*Okada et al.*, 1994; *Shinohara et al.*, 1998] and with theoretical predictions for lower hybrid drift waves. *Huba et al.* [1978] predicted fluctuations in the magnetic field of $|\delta B| \sim$ 0.09-270 pT with electric field fluctuations of $|\delta E| \sim$ 0.05-5 mV/m for the lower hybrid drift instability. The spikes in this study have $|\delta E| \sim$ 5-75 mV/m; so our values for the fluctuating magnetic field are consistent with the identification of the waves as due to the lower hybrid drift instability. For the nine events examined, there were no large-amplitude magnetic field fluctuations which could be clearly associated with the observed spiky electric fields rather than the waves. Thus the observations of the magnetic fields during the spikes are not inconsistent with the collapse mechanism.

Because the lower hybrid wave collapse mechanism would require that the spikes be embedded in a region of lower hybrid waves, the frequency of the waves observed in the raw electric field data has been compared with the local lower hybrid frequency. The data have been analyzed in 1-min segments, with a filter applied to eliminate the dc field due to the 3-s spin of the spacecraft. A fast Fourier transform of the data is taken to calculate a power spectrum, and the frequency at which the peak power occurred is then compared with the lower hybrid frequency which in this region of the magnetotail can be approximated by

$$f_{lh} = \sqrt{f_{ce} f_{ci}} \approx 0.65 B_{tot} \quad (3)$$

where B is measured in nanoteslas. This allows a direct comparison between the local lower hybrid frequency and the frequency of the waves associated with the spikes. An example of this is shown in Figure 8. The first panel shows 1-min of unfiltered raw electric

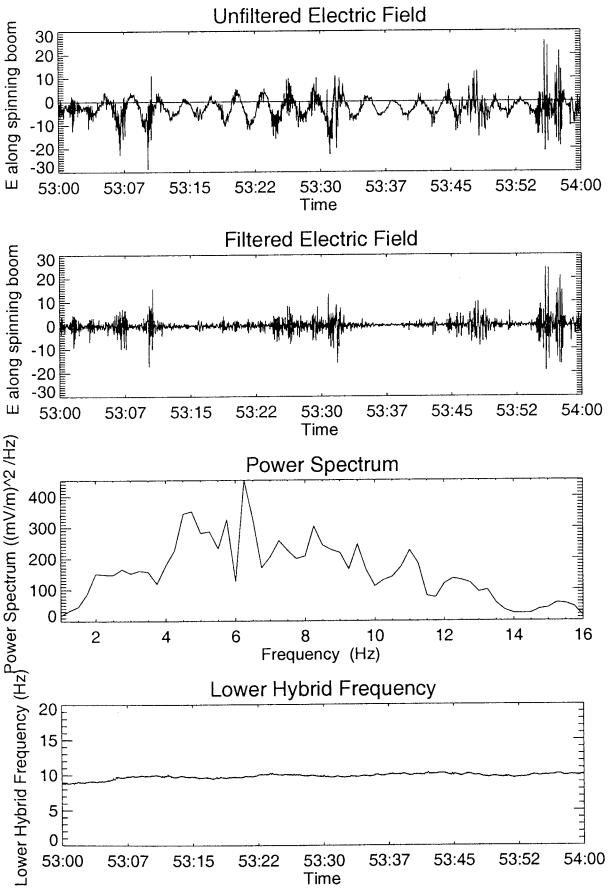

Figure 8. Frequency comparison for 1 min of data. The first panel shows the raw electric field, the second panel shows this field filtered to remove the dc offset and the 3-s spin period, the third panel shows the power spectrum of the electric field, and the fourth panel shows the lower hybrid frequency.

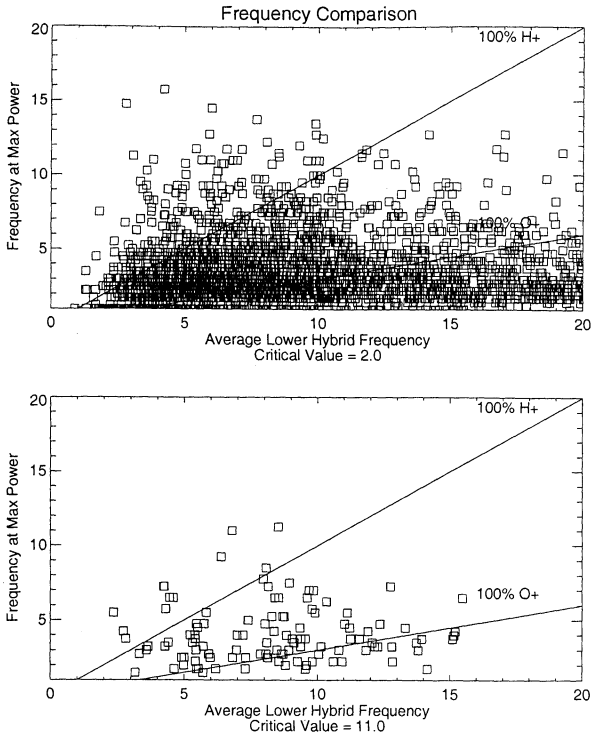

Figure 9. Comparison between the lower hybrid frequency and the frequency at maximum power for each minute within the event database. (top) Points above the critical value = 2.0 threshold. Note that most of the points lie between the lower hybrid frequency for pure hydrogen and for pure oxygen, or slightly below the lower hybrid frequency. (bottom) Electric field points with critical value > 11. Note that most of the points still lie between the lower hybrid frequency for pure hydrogen and for pure oxygen.

field (the 3-s spin period is clearly visible); the second panel shows the filtered electric field, and the third panel displays the power spectrum of the electric field. The second panel clearly shows the larger-amplitude spikes (above $\sim$ 10 mV/m) compared with the wave field. Note that the maximum power occurs near 6 Hz. The fourth panel displays the lower hybrid frequency, which is approximately 9 Hz. The result is in agreement with lower hybrid drift waves which occur at a frequency of the order of but slightly below the lower hybrid frequency [*Huba et al.*, 1978]. In the top panel of Figure 9 the frequency at maximum power is plotted versus the lower hybrid frequency for all minutes of data containing points with critical value > 2. The actual frequency depends upon the composition of the plasma. Since we did not have composition data, both extreme cases (100% oxygen and hydrogen) have been shown in the plot. Note that the vast majority of these points fall between the lower hybrid frequency for pure hydrogen and pure oxygen. Combined with the observed perpendicular polarization, the association with density gradients, and based upon previous results [*Cattell and Mozer*, 1986, 1987; *Okada et al.*, 1994; *Shinohara et al.*, 1998] of lower hybrid waves in the magnetotail, this strongly suggests that these are, in fact, lower hybrid waves. It is also interesting to examine the bottom panel of Figure 9, which shows the same data, but now for minutes of data containing points with critical value > 11, which is only the largest spikes. Again, most of the points fall between the lower hybrid frequency lines for oxygen and hydrogen.

7. Discussion

This section will examine some of the predictions of the three models discussed in section 2 to determine which are in agreement with our results. This comparison will provide a better understanding of possible generation mechanisms for these spiky electric fields.

7.1. Electrostatic and Kinetic Alfvén Wave Mapping

As was described in section 2, one of the key tests for the mapping of electrostatic shocks is whether the electric field falls off as $\sqrt{B}$ as expected under the assumption that magnetic field lines are equipotentials. This normalization was initially tested by *Levin et al.* [1983] out to radial distances of 23 R_E. This study

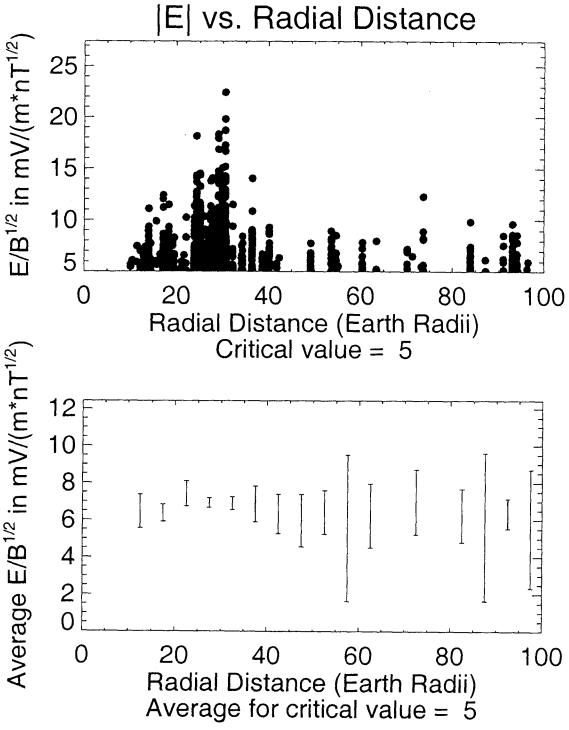

Figure 10. Plot showing magnitude of electric field points versus their corresponding radial distance, now normalized by dividing the electric field by $\sqrt{B}$. (top) All data points with critical value > 5. (bottom) Averages of all these points in 5 R_E bins. Note that even though the bottom panel indicates a fairly constant horizontal line, this result is skewed by the greater number of data points at lower values, which often occur during times when no spiky electric fields were present.

extends this test out to all regions of the magnetotail sampled by Geotail to test the mapping of electrostatic shocks theory. Figure 10 (using the same format as Figure 3) shows in the top panel the three largest electric field points per minute versus the corresponding radial distance; however, now the values of the electric field are divided by $\sqrt{B}$. This should result in a constant best fit line. The bottom panel shows 5 R_E averages of the data in the top panel. The top panel shows fairly constant amplitudes beyond 40 R_E but variable amplitudes inside this distance. Although the averages (with error bars) do fit a linear relationship, this may be misleading. Note that the averages are only slightly above 5, which is the cutoff value; thus the majority of points are barely above the cutoff criteria. Choosing a higher critical value makes the averages appear less linear and increases the size of the error bars. Thus the data in the top panel of Figure 10 are more meaningful than the averages in this case.

To help ascertain whether these spikes may be due to kinetic Alfvén waves, the data were also normalized by using the normalization condition for Alfvén waves, which can be written as

$$\text{critical value} \leq \frac{\text{spike(mV/m)} * \text{density}^{1/4}}{B} \quad (4)$$

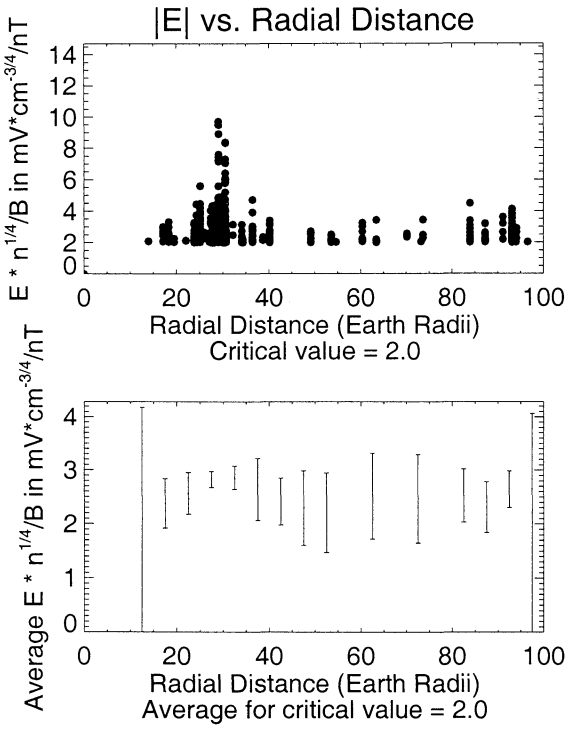

Figure 11. Plot of the magnitude of electric field points versus their corresponding radial distance, now normalized by the relationship for kinetic Alfvén waves. (top) All data points with an Alfvén critical value > 2; (bottom) averages of these results in 5 R_E bins. Again, the relationship appears fairly constant but is skewed by the excess of points at lower values, which do not correspond with times of spiky electric fields.

[R. Lysak, private communication, 1999]. Histogram plots using this normalization condition appeared similar to those shown previously, with polarizations primarily perpendicular for lower critical values, and the angles becoming oblique for larger critical values. This relationship is also plotted versus radial distance for the three largest electric field points and is shown in Figure 11. Once again, the bottom panel plots 5 R_E averages of the data in the top panel. Note that the averages are slightly above 2, which is the cutoff value; therefore the arguments made previously regarding Figure 10 apply to Figure 11 as well.

The mapping results shown above do not provide a definite test of the models, since the data agree equally well with the mapping of electrostatic shocks and kinetic Alfvén wave models. Also note that following the work of *Lysak* [1998] for kinetic Alfvén waves, one would expect magnetic fluctuations of the order of 10 pT for the electric field fluctuations seen in this study, which is slightly lower than, but not inconsistent with, the magnetic field fluctuations described above.

Wygant et al. [2000] have observed the presence of large electric fields in the plasma sheet boundary layer at altitudes of 4-6 R_E, well inside the region covered by this study. *Wygant et al.* [2000] found that the maximum electric field variations exceeded 100 mV/m, that the electric fields were oriented primarily perpendicular to the magnetic field with the dominant component perpendicular to the ecliptic (i.e., is the direction not measured by Geotail), and that these electric fields were associated with strong magnetic field fluctuations. In some cases, the phases and ratios of the electric field and magnetic field variations were consistent with propagating Alfvén waves.

7.2. Lower Hybrid Wave Collapse

The two major tests for this theory are that (from section 2.3) (1) the spikes occur in a region of lower hybrid waves and (2) the electric field amplitudes exceed the threshold condition given by equation (1). As was shown in section 6, the spikes are found within a region of lower hybrid waves, as identified by the histogram plots shown previously which show that k is primarily perpendicular to B for lower critical values, by the direct comparison of the frequency at peak power to the local lower hybrid frequency, and by their association with density gradients. In addition, it is straightforward to check the assertion of *Shapiro et al.* [1993], given by equation (1), by using a reasonable range of parameters for the plasma sheet boundary layer in the equation to find the electric field amplitudes necessary in this region of the magnetosphere for collapse to occur. This is shown in Figure 12, which shows electric field contours for various values of the total magnitude of the magnetic field and for various electron temperatures for a constant value of $k\rho_e$. For typical magnetotail densities and electron temperatures, the electric field threshold

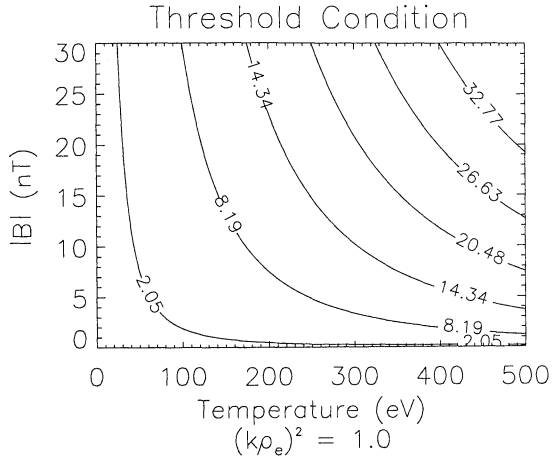

Figure 12. Contour plot for electric field amplitudes necessary for collapse according to equation (1), using reasonable values for density, frequencies, temperatures, and length scales in the magnetotail. Note that for the low density and electron temperature seen in the magnetotail, the amplitudes necessary are seen during these spiky field events.

amplitudes are equal to or less than the amplitudes of both the spiky fields and the lower hybrid waves seen during the events of this study, implying that lower hybrid wave collapse is a viable mechanism in the magnetotail, as was suggested by *Cattell et al.* [1994].

Two additional statistical results need to be discussed in the framework of the lower hybrid collapse mechanism. The first is the result that spikes are found at oblique angles to the magnetic field. *Shapiro et al.* [1993] concluded that the relevant length scales for collapse should be $L_\parallel/L_\perp > \sqrt{(M/m)}$, where M and m are the ion and electron mass, respectively. Note that the simulation of *Shapiro et al.* [1993] used $T_e/T_i = 2$ and $\omega_{pe}/\omega_{ce} = 3$, which are not applicable to the magnetotail. This result is not consistent with our results. Our data would suggest values of $L_\parallel/L_\perp$ of the order of 1. *Robinson et al.* [1996], in a review of observations of lower hybrid wave packets in density depletions at altitudes between 500 and 13,000 km, found that these results were only partially consistent with lower hybrid collapse. Observations could be explained by collapse if the lower hybrid waves either accumulated in preexisting density depletions, had multiple collapses, or produced the density depletions by a means different from the ponder motive force. The expected time and length scales in the magnetotail are much different from those in the ionosphere, as are many of the parameters used in lower hybrid collapse simulations; so the expected ratio of $L_\parallel/L_\perp$ for lower hybrid collapse in the magnetotail is not precisely known. The electric field detector on Geotail does not provide the needed resolution to measure an individual collapsing cavity, only measuring larger scales containing multiple cavities. Thus we can only determine the cavity shape statistically. The second result is the lack of spiky electric field events beyond 100 R_E. This result may be consistent with the collapse mechanism, as can be seen by noting that electric field amplitudes fall off with radial distance (see Figure 3) and that electric field values are below the threshold condition of equation (1) for distances downtail beyond ~ 100 R_E.

The presence of lower hybrid waves in the same region as the spikes and the fact that the observed electric fields are above threshold amplitudes for collapse all point to lower hybrid wave collapse as the leading candidate for the generation mechanism for these structures.

8. Conclusions

The Geotail data set provides an excellent opportunity to perform an in-depth statistical study of spiky electric fields in all regions of the magnetotail. The study described herein led to the following conclusions regarding these fields and their origin.

Spikes are found throughout the magnetotail plasma sheet, but none are found beyond 100 R_E. This is consistent with the hypothesis that these fields do not occur beyond the distant x line. The fact that large spikes (as large as 100 mV/m) and lower hybrid waves occur primarily during periods of high magnetic activity suggests that they are of dynamic importance in the magnetotail. *Cattell and Mozer* [1986, 1987] have suggested that the lower hybrid waves and spiky fields may be important in dissipation. Spiky fields are embedded in regions of lower hybrid waves, as identified by the polarization histogram plots which show that the electric field lies primarily perpendicular to the magnetic field, by comparing the frequency at peak power to that expected for lower hybrid drift [*Huba et al.*, 1978], and by the association with density gradients. By examining cases with larger electric field amplitudes, i.e., analyzing the spikes and not the lower hybrid waves with which they are collocated, it is found that the spikes more frequently occur at angles which are oblique to the magnetic field. For reasonable values of the temperature and density for the plasma sheet, the condition for lower hybrid wave collapse given by *Shapiro et al.* [1993] results in wave electric field amplitudes consistent with those observed during the spiky field events in this study.

Tests of normalizations for the mapping of electrostatic shocks and kinetic Alfvén waves were shown to be inconclusive, in that the data roughly fit both normalization schemes. This suggests that normalization testing is not an effective method for differentiating between generation mechanisms over this altitude range.

The facts that the spikes are found in regions with lower hybrid waves, that wave amplitudes are large enough for collapse to occur, and that the predominance of oblique angles does not match the mapping of electrostatic shocks, which are mostly perpendicular, strongly suggest that these spikes are related to lower hybrid drift wave collapse [*Shapiro et al.*, 1993]. Note that re-

cent studies have suggested that some low-altitude observations do not fit simple collapse models [*Robinson et al.*, 1996]; however, since magnetotail parameters are much different from those in the ionosphere, their arguments may not be valid for our case.

Further work will continue to shed more light on spiky electric fields and their impact on magnetotail dynamics. Definite identification of the generation mechanism and the role of collapse in the magnetotail will require a full three-dimensional measurement of the electric field and simultaneous high time resolution electric and magnetic field data which will not be available until the Magnetospheric Multiscale Mission. Theoretical and simulation work should continue to examine the lower hybrid collapse mechanism, specifically for magnetotail parameters.

Simulation work using a particle tracing code has shown the inclusion of lower hybrid waves in the magnetotail has a large effect on particle trajectories and energization [*Cattell et al.*, 1995a, T. Streed et al., manuscript in preparation, 2001]. Preliminary results have also shown that including an analytical model of the spikes, based upon these Geotail statistics, results in large modification to particle trajectories and energization and changes in particle distributions in both configuration and velocity space. This is consistent with previous studies of effects of spikes on electrons [*Temerin and Cravens*, 1990] and ions [*Borovsky*, 1984] in the auroral zone. Work will continue in this area.

Acknowledgments. Thanks to Jack Vernetti at UC Berkeley for his valuable work on the data analysis software and to the ISAS/Darts system for the magnetic field data. This work was supported by NSF grant ATM-9506594. Work at UC Berkeley was supported by NAGS-2718. C. Cattell is a Cotrell Scholar.

Hiroshi Matsumoto thanks the referees for their assistance in evaluating this paper.

References

Borovsky, J., The production of ion conics by oblique double layers, *J. Geophys. Res.*, *89*, 2251, 1984.

Cattell, C., and F. Mozer, Electric fields measured by ISEE-1 within and near the neutral sheet during quiet and active times, *Geophys. Res. Lett.*, *9*, 1041, 1982.

Cattell, C., and F. Mozer, Experimental determination of the dominant wave mode in the active near-earth magnetotail, *Geophys. Res. Lett.*, *13*, 221, 1986.

Cattell, C., and F. Mozer, Substorm-associated lower hybrid waves in the plasma sheet observed by ISEE 1, in *Magnetotail Physics*, edited by A. Lui, AGU, Washington, D.C., 1987.

Cattell, C., M. Kim, R. Lin, and F. Mozer, Observations of large electric fields near the plasma sheet boundary by ISEE-1, *Geophys. Res. Lett.*, *9*, 539, 1982.

Cattell, C., F. Mozer, K. Tsuruda, H. Hayakawa, M. Nakamura, T. Okada, S. Kokubun, and T. Yamamoto, Geotail observations of spiky electric fields and low-frequency waves in the plasma sheet and plasma sheet boundary, *Geophys. Res. Lett.*, *21*, 2987, 1994.

Cattell, C., I. Roth, and M. Linton, The effects of low frequency waves on ion trajectories in the Earth's magnetotail, *Geophys. Res. Lett.*, *22*, 3445, 1995a.

Cattell, C., J. Wygant, F. Mozer, T. Okada, T. Tsuruda, S. Kokubun, and T. Yamamoto, ISEE 1 and Geotail observations of low-frequency waves at the magnetopause, *J. Geophys. Res.*, *100*, 11,823, 1995b.

Cattell, C., et al., Effects of low frequency waves and spiky electric fields in the magnetotail, in *Proceedings of the Third International Conference on Substorms (ICS3)*, Versailles, France, 1996.

Huba, J., N. Gladd, and K. Papadopoulos, Lower hybrid drift wave turbulence in the distant magnetotail, *J. Geophys. Res.*, *83*, 5217, 1978.

Ishisaka, K., T. Okada, Y. Kasaba, F. Mozer, K. Tsuruda, H. Matsumoto, and H. Hayakawa, Electron temperature and density of magnetospheric plasma from GEOTAIL spacecraft potentials, *Adv. Space Res.*, *24, 1*, 129, 1999.

Kokubun, S., T. Yamamoto, M. Acuna, K. Hayashi, K. Shiokawa, and H. Kawano, The Geotail magnetic field experiment, *J. Geomag. Geoelectr.*, *46*, 7, 1994.

Levin, S., K. Whitley, and F. Mozer, A statistical study of large electric field events in the Earth's magnetotail, *J. Geophys. Res.*, *88*, 7765, 1983.

Louarn, P., J. Wahlund, T. Chust, H. de Feraudy, A. Roux, B. Holback, P. Dovner, A. Eriksson, and G. Holmgren, Observation of kinetic Alfvén waves by the FREJA spacecraft, *Geophys. Res. Lett.*, *21*, 1847, 1994.

Lysak, R., The relationship between electrostatic shocks and kinetic Alfvén waves, *Geophys. Res. Lett.*, *25*, 2089, 1998.

Lysak, R., and C. Dum, Dynamics of magnetosphere-ionosphere coupling including turbulent transport, *J. Geophys. Res.*, *88*, 365, 1983.

Lysak, R., and W. Lotko, On the kinetic dispersion relation for shear Alfvén waves, *J. Geophys. Res.*, *101*, 5085, 1996.

Matsumoto, H., H. Kojima, Y. Omura, and I. Nagano, Plasma waves in geospace: GEOTAIL observations, in *New Perspectives on the Earth's Magnetotail, Geophys. Monogr. Ser.*, edited by A. Nishida, D. Baker, and S. Cowley, vol. 105, AGU, Washington, D. C., 1998.

McFadden, J., C. Carlson, and R. Ergun, Microstructure of the auroral acceleration region as observed by FAST, *J. Geophys. Res.*, *104*, 14,453, 1999.

Mozer, F., ISEE-1 observations of electrostatic shocks on auroral zone field lines between 2.5 and 7 Earth radii, *Geophys. Res. Lett.*, *8*, 823, 1981.

Mozer, F., and C. Kletzing, Direct observations of large, quasi-static, parallel electric fields in the auroral acceleration region, *Geophys. Res. Lett.*, *25*, 1629, 1998.

Mozer, F., C. Carlson, M. Hudson, R. Torbert, B. Parady, J. Yatteau, and M. Kelley, Observations of paired electrostatic shocks in the polar magnetosphere, *Phys. Rev. Lett.*, *38*, 292, 1977.

Nishida, A., The Geotail mission, *Geophys. Res. Lett.*, *21*, 2871, 1994.

Okada, T., et al., Geotail observations of electrostatic waves in the lower hybrid frequency range in the plasma sheet boundary layer, *Geophys. Res. Lett.*, *21*, 2931, 1994.

Pedersen, A., Solar wind and magnetosphere plasma diagnostics by spacecraft electrostatic potential measurements, *Ann. Geophys.*, *13*, 118, 1995.

Redsun, M., M. Temerin, and F. Mozer, Classification of auroral electrostatic shocks by their ion and electron associations, *J. Geophys. Res.*, *90*, 9615, 1985.

Robinson, P., A. Melatos, and W. Rozmus, Is there lower hybrid wave collapse at auroral latitudes?: Theory versus observations, *J. Geophys. Res.*, *101*, 21,545, 1996.

Shapiro, V., V. Shevchenko, G. Solov'ev, V. Kalinin, R. Bingham, R. Sagdeev, M. Ashour-Abdalla, J. Dawson,

and J. Su, Wave collapse at the lower-hybrid resonance, *Phys. Fluids B*, *5*, 3148, 1993.

Shinohara, I., T. Nagai, M. Fujimoto, T. Terasawa, T. Mukai, K. Tsuruda, and T. Yamamoto, Low-frequency electromagnetic turbulence observed near the substorm onset site, *J. Geophys. Res.*, *103*, 20,365, 1998.

Temerin, M., and D. Cravens, Production of electron conics by stochastic acceleration parallel to the magnetic field, *J. Geophys. Res.*, *95*, 4285, 1990.

Temerin, M., and F. Mozer, Double layers above the aurora, *Laser Particle Beams*, *5*, 203, 1987.

Tsuruda, K., H. Hayakawa, M. Nakamura, T. Okada, A. Matsuoka, F. Mozer, and R. Schmidt, Electric field measurements on the Geotail satellite, *J. Geomag. Geoelectr.*, *46*, 693, 1994.

Wygant, J., M. Bensadoun, and F. Mozer, Electric field measurements at oblique subcritical bow shocks, *J. Geophys. Res.*, *92*, 11,109, 1987.

Wygant, J., et al., Polar spacecraft-based comparisons of intense electric fields and Poynting flux near and within the plasma sheet-tail lobe boundary to UVI images: An energy source for the aurora, *J. Geophys. Res.*, *105*, 18,675, 2000.

C. Cattell and T. Streed, School of Physics and Astronomy, University Of Minnesota, 116 Church St. S.E., Minneapolis, MN, 55455. (cattell@fields.space.umn.edu; tstreed@fields.space.umn.edu)

S. Kokubun, STELAB, Nagoya University, Toyokawa 442, Japan.

F. S. Mozer, Space Sciences Laboratory, University of California, Berkeley, CA 94720.

K. Tsuruda, ISAS, Sagamihara 229, Japan.

(Received February 9, 2000; revised November 2, 2000; accepted November 2, 2000.)